

Fatigue monitoring and maneuver identification for vehicle fleets using the scattering transform

L. Heindel^a, P. Hantschke^{a,b}, M. Kästner^{a,b,*}

^a*Technische Universität Dresden, Institute of Solid Mechanics, 01062 Dresden, Germany*

^b*Dresden Center for Fatigue and Reliability (DCFR), 01062 Dresden, Germany*

Abstract

Extensive monitoring comes at a prohibitive cost, limiting Predictive Maintenance strategies for vehicle fleets. This paper presents a measurement-based soft sensing technique where local strain gauges are only required for few reference vehicles, while the remaining fleet relies exclusively on accelerometers. The scattering transform is used to perform feature extraction, while principal component analysis provides a reduced, low dimensional data representation. This enables direct fatigue damage regression, parameterized from unlabeled usage data. Identification measurements allow for a physical interpretation of the reduced representation. The approach is demonstrated using experimental data from a sensor equipped eBike.

Keywords: predictive maintenance, fatigue monitoring, maneuver identification, scattering transform, soft sensing

1. Introduction

Engineering vehicles against fatigue failure is a complex problem, which consists in a comparison between the fatigue strength of the vehicle components and the expected operational loads during the lifetime of the vehicle. Many load assumptions have to be made, in order to generate a representative load collective, which reflects the expected regular usage scenarios and simultaneously takes special events into account. A detailed summary of both established procedures, as well as novel approaches in this field, is given in BURGER et al. [1]. Once a design is finished, the probability of failure for an individual component, with respect to the chosen load collective, is known. However, the particular load history, which any individual vehicle experiences during its service life, is generally not known. This is a significant challenge for the estimation of its remaining useful life time.

The aim of predictive maintenance is to identify accumulating damage in critical components preemptively, i.e. before failure occurs, in order to schedule replacements by demand. This allows to better exploit real load bearing capabilities and to prevent system failures. Numerous existing works in the field of structural health monitoring (SHM) address this problem by monitoring system responses with the aim of detecting changes in the system behavior and thus inferring component damage. A detailed review of classical approaches in SHM for civil infrastructure is given by BROWNJOHN [2], while a review of recent approaches involving machine learning algorithms is provided in [3]. The approach of detecting changes in the system behavior is feasible, since buildings are generally designed in a redundant manner, where the failure of an individual substructure does not cause an immediate collapse of the entire structure. Motor vehicles, however, are generally build with lightweight design in mind. While a variety of crash scenarios are taken into account for reasons of passenger safety, the failure of individual components can immediately impair the roadworthiness of the vehicle. Damage due to material fatigue accumulates over a long period of time and can occur very abruptly when a critical damage threshold is reached. As a result, detecting changes in the

*Corresponding author. E-mail: Markus.Kaestner@tu-dresden.de ; Tel.: +49 351 463-43065 ; fax: +49 351 463-37061.

system behavior can be too reactive for many applications.

A predictive maintenance approach for these applications should therefore monitor the load history at critical components in a system, in order to provide information about the fatigue damage accumulation. To conduct a fatigue damage calculation following established procedures [4], local strain or stress information is required. The installation of a sufficient number of sensors, e.g. strain gauges, for such an elaborate monitoring is, however, uneconomic and impractical in many applications and therefore usually limited to prototypes in the design process or designated measuring vehicles, as described in STELLMACH et al. [5]. This is unfortunate, since service and repair of consumer vehicles could benefit immensely from such monitoring.

Frequency based fatigue life estimation methods [6] are commonly used in the automotive industry, since they are suited for stationary Gaussian loadings, resulting from a combustion engine and random underground excitation. A promising approach is provided by UGRAS et al. [7], where the fatigue life of truck components is monitored through acceleration measurements, using frequency response functions obtained by finite element simulations and frequency domain methods for fatigue estimation, implemented as an on board solution. Other possible solutions to this problem are given by virtual sensing (VS) or soft sensing approaches, which approximate unmeasured system responses or related quantities of interest based on available measurement data. This enables system monitoring through reduced sensor configurations and provides solutions in situations where quantities of interest are difficult to measure or sensor locations are inconvenient to access. Virtual sensing approaches can be fundamentally divided into model-based and data-based approaches.

Model-based strategies are characterized by the presence of a physics based model, which describes the relationship between the system response of interest and the measurable quantities. Examples from this category are commonly methods based on finite element simulations and experimental modal analysis. HJELM et al. [8] shows that stress histories can be obtained indirectly from strain measurements using a physical VS model, which is shown using experimental measurements from a lattice tower. Similar approaches, which also employ the combination of finite element simulation and modal analysis, are provided by TARPO et al. [9] and FLORES TERRAZAS et al. [10], where VS is used to enable fatigue monitoring of an offshore structure and wind turbine tower, respectively. In the field of motor vehicles, physical modeling approaches like the finite element method can be costly to parameterize and obtaining accurate predictions for highly dynamic and non-linear systems is generally very resource intensive.

In contrast, data-based approaches rely on existing datasets, which contain the relationship between measurements and responses implicitly. A variety of machine learning approaches exist in this field. In ROUSS et al. [11], an artificial neural network is employed to predict the behavior of a non-linear dynamic system, which is demonstrated using measurements from a vibrating platform. KULLAA [12, 13] presents various methods for both model- and data-based virtual sensing, e.g. estimating redundant sensors in a network, reducing measurement noise and providing full field information from a limited set of sensors. Data driven VS is also employed for audio transmission in WANG et al. [14], where noise signals at the passenger ear side are reconstructed from audio measurement at different locations in the interior. During the parameterization phase, these methods require measurements of the system response of interest. Once the system is deployed, these measurements are no longer required and instead replaced by data-based predictive models.

The aim of this paper is to provide an economic soft sensing approach for fatigue damage monitoring of vehicle fleets, which can be parameterized using only measurement data. It is based on a low dimensional data representation, which is obtained by a combination of feature extraction and dimensionality reduction. Here, the scattering transform provides a powerful tool for the extraction of fatigue related information, leading to two separate applications, namely fatigue damage regression and maneuver identification. A sensor-equipped eBike serves as a demonstrator for the presented approach, with which an experimental dataset was acquired.

The paper is structured as follows: First, necessary fundamentals of the presented approach, i.e. Scattering Transformation and PCA are presented. On this basis, the low-dimensional data representation is elaborated. Subsequently, the experimental setup is presented and the resulting data sets are described in detail. As the first application, an approach for direct damage monitoring using a reduced sensor configuration is presented. Secondly, the data representation is used in a discrete maneuver identification example. After-

wards, the most essential results of this study are evaluated and discussed. The paper concludes with a short summary and an outlook on possible extensions and improvements of the presented methods.

2. Material and Methods

In this paper, a combination of the scattering transform and principal component analysis (PCA) is used to extract and compress useful sensor information. In the following explanations, vectors \underline{v} and matrices $\underline{\underline{M}}$ are denoted by single and double underscores, respectively.

2.1. Fourier and Wavelet transform

Given a time series $x(t)$, the Fourier transform of this time series

$$\hat{x}(\omega) = \int_{-\infty}^{\infty} x(t)e^{-i2\pi\omega t} dt \quad (1)$$

describes the frequency content of $x(t)$, but does not include information about the specific point in time, at which an observed frequency occurred. Since many applications exist, where information from both time and frequency domains plays an important role, additional analysis tools were developed. The Short Time Fourier transform (STFT) computes the Fourier transform of signals over small time windows, leading to a spectrogram which displays frequency and time information simultaneously with homogeneous resolution. In a similar manner, the continuous wavelet transform (CWT) is obtained by computing the correlation

$$x_{\psi}(a,b) = \frac{1}{|a|^{\frac{1}{2}}} \int_{-\infty}^{\infty} x(t)\overline{\psi\left(\frac{t-b}{a}\right)} dt = \frac{1}{|a|^{\frac{1}{2}}} x(t) \star \overline{\psi_{a,b}(t)} \quad (2)$$

between $x(t)$ and a wavelet basis

$$\psi_{a,b}(t) = \psi\left(\frac{t-b}{a}\right), \quad (3)$$

which is constructed from a mother wavelet $\psi(t)$ using a dilation factor a and a shifting parameter b . The operator \star refers to the correlation operator

$$f(\tau) \star g(\tau) = \int_{-\infty}^{\infty} f(\tau)\overline{g(t+\tau)} dt. \quad (4)$$

The CWT results in a scalogram, which is similar to the spectrogram in the sense that it contains information in the frequency and time domain. The main difference is that scalogram leads to an adaptive resolution, where low frequencies in $x(t)$ are resolved with a high resolution in the frequency domain, but a low resolution in time, and high frequencies in $x(t)$ feature a high resolution in the time domain and a low resolution in frequency.

2.2. Scattering transform

The Scattering transform, introduced in [15, 16, 17], extracts signal invariants from a time series in order to provide useful features to discriminate between different classes of signals, i.e., a classification task. It has been employed in different temporal and spacial classification problems, where similar results to state of the art deep neural network approaches were achieved without necessitating a data intensive training process. In SEYDOUX et al. [18], it provides the basis for an unsupervised clustering framework which detects seismic signals. The transform is explained in great detail in [16] and only briefly reviewed here.

The architecture of the scattering transform is depicted in Figure 1. It bears many similarities to convolutional neural networks and is designed to extract features from $x(t)$, which are both translation invariant

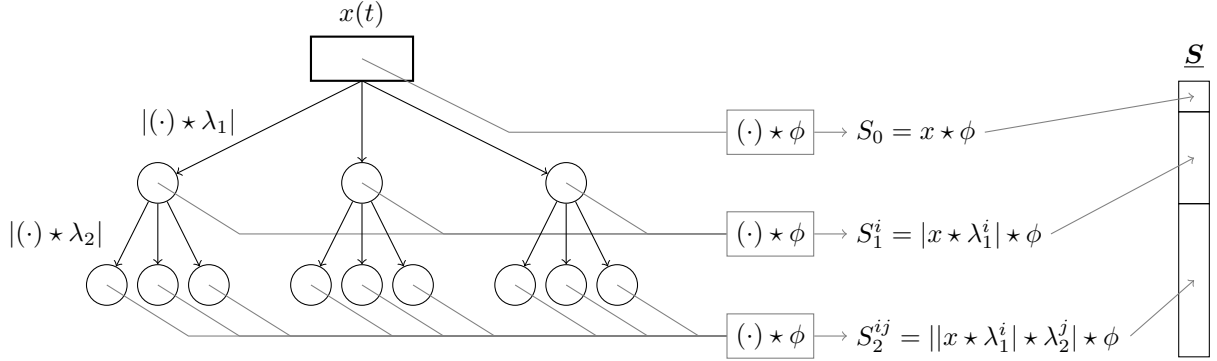


Figure 1: The scattering transform applies multiple layers of wavelet convolutions $(\cdot) \star \lambda_w$ and modulus operations $|(\cdot)|$ to an input signal $x(t)$. The vector of scattering coefficients \underline{S} is structured in sections corresponding to each layer. These sections contain an entry per dilated wavelet, time averaged via a low pass filter ϕ .

and stable to time warping deformation. This is achieved by iteratively computing multiple layers of wavelet convolutions $(\cdot) \star \lambda_w$ and modulus operations $|(\cdot)|$, where the index w denotes the layer index.

The wavelet basis used in the first scattering layer λ_1 is similar to the basis $\psi_{a,b}(t)$ introduced in Equation 3 in the sense that a mother wavelet $\psi(t)$ is dilated

$$\psi_{\lambda_1}(t) = \lambda_1 \psi(\lambda_1 t), \quad (5)$$

by a set of dilation factors

$$\lambda_1 \in \{2^{k/Q} | k \in \mathbb{Z}\}, \quad (6)$$

defined by a given number of wavelets per octave Q . Afterwards, a modulus operation is applied and the first layer of the transform $|x(t) \star \lambda_1|$ is complete. The information contained in this layer is similar to the information in a spectrogram or scalogram.

For the next layer, the process is repeated iteratively using the wavelet basis

$$\psi_{\lambda_2}(t) = \lambda_2 \psi(\lambda_2 t), \quad (7)$$

which can be different from ψ_{λ_1} . While more than two scattering layers can be computed, two layers are sufficient for most practical signal classification tasks. In order to achieve translation invariance in the scattering coefficients, the outputs of each layer are averaged in time by correlation with a low pass filter ϕ , whose averaging scale is given by 2^J with $J \in \mathbb{N}$. The vector of coefficients \underline{S} is composed of the time averaged outputs of each scattering layer, resulting in a hierarchical structure with an increasing number of coefficients per layer.

In this paper, the Python library Kymatio [19] is used to compute the scattering transform. Apart from the parameters J and Q , which define the wavelet basis of the transform, the length in time T of the mother wavelet can also be specified. In this software environment, the mother wavelet shape is fixed to complex valued Morlet Wavelets.

2.3. Principal component analysis

Principal component analysis (PCA) [20] is an orthogonal, linear coordinate transformation, which describes a dataset by a new basis, ordered by variance. It is commonly used for dimensionality reduction and has become a common tool in data science and engineering.

In the context of PCA, a dataset is given by a data matrix \underline{D} , in which data samples \underline{d} are arranged in rows and the columns are comprised of the features of each sample. The aim of principal component analysis is to

represent \underline{D} in the principal component space \underline{H} , where the first principal axis lies in the direction of highest variance in \underline{D} . For each subsequent principal axis, their variance is maximized under the condition that it is orthogonal to all previous principal axes. This is achieved by applying an orthogonal transformation \underline{U} , so that

$$\underline{H} = \underline{D}\underline{U}. \quad (8)$$

It can be shown that the columns of the transformation matrix \underline{U} are the eigenvectors \underline{u} of $\underline{D}^T \underline{D}$, ordered by the size of their eigenvalues. These eigenvectors \underline{u} can also be obtained via a singular value decomposition of the data matrix \underline{D} , which is the standard way of computing \underline{U} . Transforming a data sample \underline{d} into principal component space

$$\underline{h} = \underline{d}\underline{U} \quad (9)$$

simply describes it as a weighted sum of eigenvectors \underline{u} , where the weights \underline{h} of these eigenvectors are called principal component (PC) scores. Given the PC scores \underline{h} , the original data sample can be reconstructed

$$\underline{d} = \underline{h}\underline{U}^T \quad (10)$$

since \underline{U} is orthogonal. A dimensionality reduction can be achieved by simply truncating the transformation matrix

$$\underline{H}_{\text{red}} = \underline{D}\underline{U}_{\text{red}} \quad (11)$$

and discarding the PC axes below a selected variance threshold θ . Because the principal axes in \underline{H} are ordered by variance, in most examples using real world data, the first eigenvectors $\underline{u}_{1,\dots,\theta-1}$ contribute significantly more to the reconstruction of \underline{d} than the discarded low variance eigenvectors. Using this reduced transform, a datapoint d can be represented by the PC scores of the truncated basis

$$\underline{h}_{\text{red}} = \underline{d}\underline{U}_{\text{red}} \quad (12)$$

which is described as dimensionality reduction, since the number of elements in $\underline{h}_{\text{red}}$ can be significantly lower than the dimensionality of d , while still achieving a low reconstruction error

$$\underline{d}_{\text{red}} = \underline{h}_{\text{red}}\underline{U}_{\text{red}}^T \approx \underline{d} \quad (13)$$

depending on the particular dataset and the chosen threshold θ .

PCA computations in this work are carried out using the Python library Scikit-Learn [21]. Since an important requirement of PCA is that each feature has a mean of zero, the feature-wise mean over all samples in \underline{D} is computed and subtracted before the PCA is applied.

3. Experiments

This paper demonstrates novel fatigue monitoring methods, which are parameterized and validated using a dataset of eBike measurements.

3.1. Experimental setup and data

Experimental data is collected using the instrumented eBike of the brand Nuvelos, depicted in Figure 2. Its frame is equipped with 5 uniaxial acceleration sensors and 16 strain gauges. One sensor of each type is shown exemplarily in Figure 3.

While driving, the sensor data of all acceleration and strain channels is processed synchronously using two measurement amplifiers, located in the box on the rear rack. The data is then forwarded to a laptop and recorded with a sampling frequency of 1200 Hz. The only preprocessing step consists in removing data at the start and end of each file where the measurement is being started, but the eBike is not yet in motion.

During the conducted measurement rides and maneuvers, roughly half of the of the strain sensor channels exhibited fatigue critical strain amplitudes. In order to keep the presented results clear and compact, the remaining strain sensors are omitted in the following investigations.

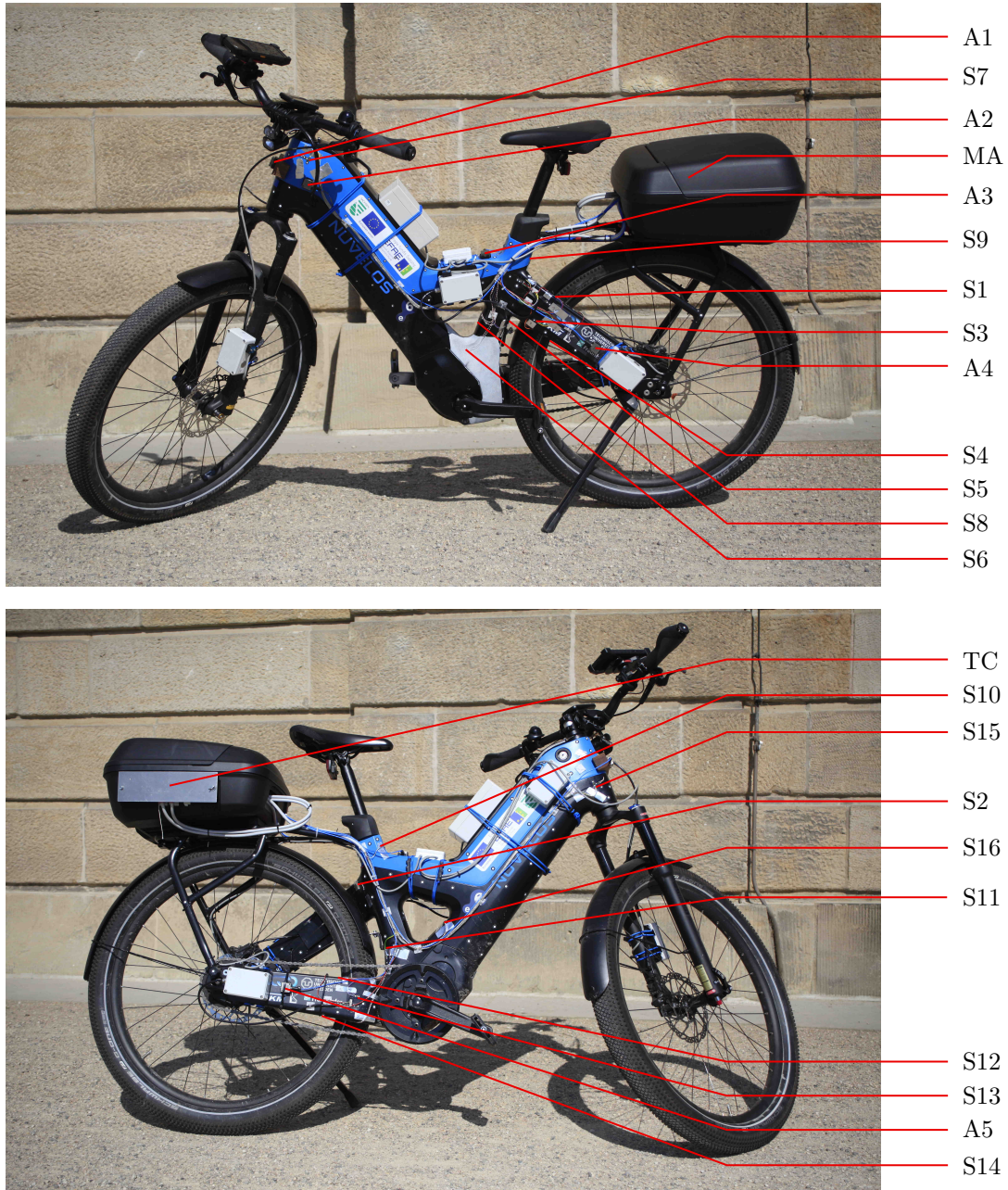


Figure 2: The measurement eBike is equipped with a variety of sensors. Their detailed locations are marked with "A" for acceleration sensors and "S" for strain gauges. The measurement amplifier is labeled as "MA", while "TC" refers to the temperature compensation gauges, which are attached to the side of the measurement box on a piece of fibre reinforced Bike frame material. The white boxes contain a different sensor setup which is not used in this study.

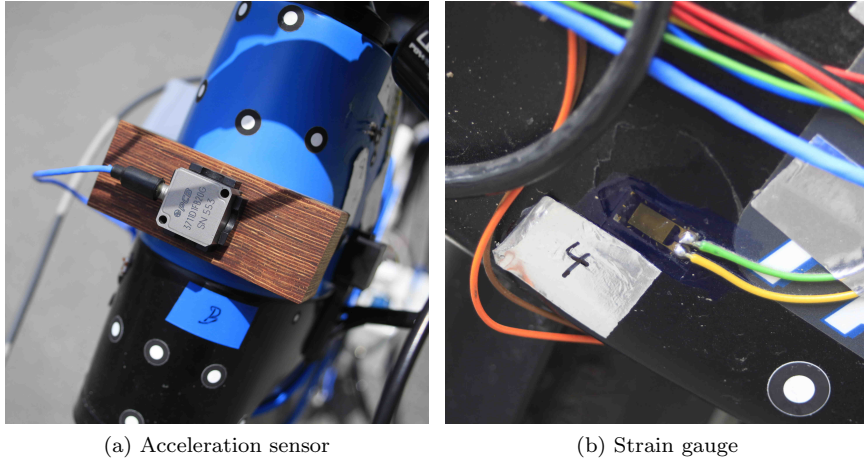


Figure 3: The sensor setup contains a total of 5 acceleration sensors (a) and 16 strain gauges (b).

3.1.1. Unlabeled usage data

The unlabeled dataset includes regular eBike usage data from three different riders. For each individual data file, only the corresponding rider is known, but information on the precise order of events during the ride and the exact route are not available. It features various ordinary driving undergrounds like roads and bike paths, as well as park and forest trails. Since medium to high electric assistance of the eBike was used during most of the rides, the riding speed is mostly in the range of 20 km/h to 25 km/h. The respective weights of the individual riders are 66 kg for rider 1, 83 kg for rider 2 and 110 kg for rider 3. This dataset contains 26 files with an individual length between 3 and 32 minutes, totaling 5.1 hours of unlabeled data.

3.1.2. Labeled data

In addition to the general eBike usage data, specific driving situations were measured. In this second, smaller dataset, each measurement file only contains data on one specific underground with a specified velocity. Information about the rider, the underground and the target velocity is available as labels to the file. While the riding speed was controlled manually during these measurement rides, the respective target speed could still be maintained within a limit of ± 1.5 km/h.

The labeled dataset includes an even asphalt underground and a very uneven cobblestone surface. For both undergrounds, measurements were taken in two different locations in order to provide independent data for model parameterization and testing purposes. For the first asphalt location, depicted in Figure 4 a), measurements at 5, 10, 15, 20 and 25 km/h are available. The second asphalt location, see Figure 4 b), was slightly more restricted, therefore only measurements from 5 to 20 km/h were collected. For both cobblestone measurement sites, depicted in Figure 4 c) and d), measurements at 5, 10 and 15 km/h are available. This measurement program was collected in identical fashion for both rider 1 and rider 2, while no labeled data is available for rider 3.

3.1.3. Data processing workflow

The data processing workflow provided by this work is targeted at information monitoring for predictive maintenance. Regarding a fleet of many identical vehicles, this can be efficiently achieved by selecting a single vehicle as a reference, which is equipped with acceleration and strain sensors. Both types of sensors are required for model parameterization, since a relationship between acceleration and strain data has to be established. During model deployment, predictions are made based on only acceleration sensors, leading



Figure 4: Labeled measurements on even underground where collected in location (a) and (b), while uneven cobblestone underground measurements were conducted at locations (c) and (d). In order to avoid dependencies in the sensor data between training (a,c) and testing (b,d) different measurement sites were used for the same underground type.

to a reduced sensor setup for all remaining standard vehicles. The sensor equipped eBike, introduced in Subsection 3.1, serves as the demonstrator for this approach.

The overall structure of the workflow consists of time series segmentation, the application of a data transformation and lastly, dimensionality reduction. While the scattering transform is specifically designed to extract features from signal which are relevant for classification, it can be substituted with different data transforms, according to the problem at hand. In order to compare the scattering transform to an established standard, most application examples are repeated using the Fast Fourier transform, which is generally easier to implement and interpret.

The entire data processing workflow is depicted in Figure 5. Experimental acceleration data is obtained in the form of $n_{\text{ch}} = 5$ channels of measurement time series with uniform sampling rate. The data is first split into shorter, non overlapping sequences called data samples, which each contain $l_{\text{seq}} = 4096$ data points. Each data sample spans a duration of 3.4 s, given the sampling rate of 1200 Hz. Afterwards, the chosen data transformation is applied individually to each time series segment and each measurement channel. For the scattering transform, a scale exponent of $J = 5$ and a number of octaves $Q = 6$ are used, which were selected through preliminary test cases. The input sequences of the Fast Fourier transform are each multiplied with a Hamming window of equal length in order to avoid discontinuities at the start and end of each sample. After computing the transformation, the coefficients of all measurement channels corresponding to one data sample are assembled in a coefficient vector. After all measurement files are processed, the complete processed data is organized in a coefficient matrix, where the columns contain the individual transformation coefficients of all channels and each row represents a data sample from a time series segment.

This data matrix will be used to parameterize the principal component analysis algorithm in order to obtain a dimensionality reduction. As preprocessing, the data is first standardized separately in each channel and in the case of the scattering transform, individually for each scattering layer. Then, the mean of the data matrix is subtracted and the PCA is applied. This requires deciding how many principal axes to keep in the truncated basis $\underline{h}_{\text{red}}$ by choosing a suitable variance cutoff θ . As shown in Figure 6, a cutoff of at least 0.2% of the total variance per axis was chosen, leading to 9 principal axes in the case of the scattering transform

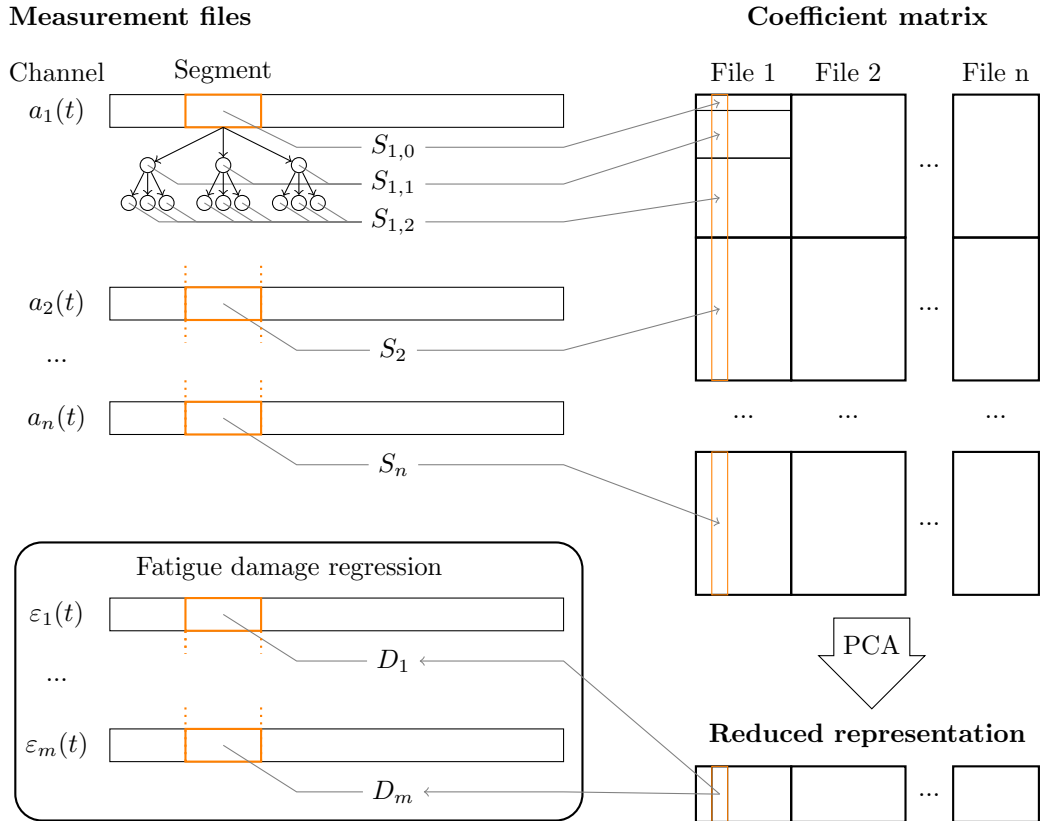


Figure 5: Each measurement file is composed of acceleration sensor channels $a_i(t)$ and strain gauge channels $\varepsilon_j(t)$. Inside a single file, the time series data is processed in sequences. From the acceleration measurements, scattering or Fourier coefficients are computed and stored in the coefficient matrix, which is displayed in transposed form for illustrative purposes. Principal component analysis is then used to transfer the coefficient information to a reduced, low dimensional representation, where each segment is now described by a limited set of principal component scores. This reduced representation provides the basis for fatigue monitoring applications. It can be used to directly predict fatigue damage sums D_j for corresponding segments of the strain channels ε_j or to predict maneuver categories using the labeled dataset.

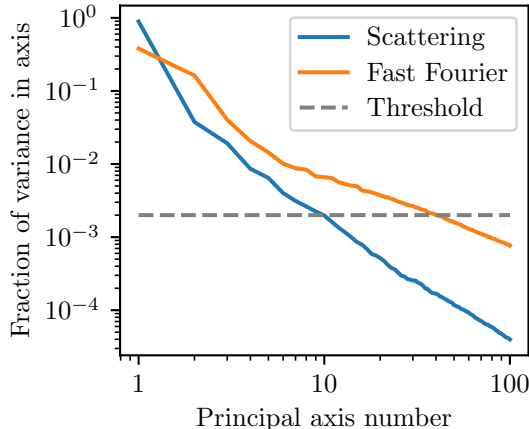


Figure 6: The variance content in each principal axis is steadily decreasing with each additional component. The variance content in the first principal axis is higher for the scattering based approach, followed by a steep descent. In order to achieve a dimensionality reduction, a cutoff was performed at 0.2% of total variance per component.

and 40 principal axes for the FFT based model. Compared to the full basis, the remaining axes amount to 97.7% of the original variance for the scattering transform and 76.2% for the Fast Fourier approach. While the FFT based model clearly loses information between transformation and PCA, obtaining the same 97.7% as the scattering variant would require keeping about 1000 principal axes. This defeats the purpose of a low dimensional representation and would cause issues with many commonly used regression and classification algorithms.

After applying both data transformation and PCA, each sample is now described only by a set of 9 or 40 principal component scores, depending on the transformation, as opposed to the original acceleration measurements of 5 sensor channels with 4096 data points per sample. This compression of sensor information enables fatigue damage regression and maneuver classification applications by operating directly on the principal component scores.

4. Fatigue monitoring

The aim of this application is to showcase how the measurements of only acceleration sensors can be used to monitor the fatigue damage accumulation at the strain sensor locations.

4.1. Regression setup

While a reduced data representation is only computed from the acceleration data samples, the simultaneously measured sequences of the strain gauges are used to link the reduced acceleration information to a corresponding fatigue damage. In this example application, this is achieved by a fictitious damage calculation following the nominal stress concept [4]. While stress data is not accessible directly, a proportionality of nominal stresses and local strains is assumed. The strain sequences are first rainflow cycle counted using the second pass of the 4-point algorithm [22], leading to a rainflow matrix $\underline{\underline{M}}_{\text{RF}}$ and avoiding influences of a resulting residuum. In order to relate the strain hystereses in $\underline{\underline{M}}_{\text{RF}}$ to an endured number of load cycles N , a fictitious WÖHLER-curve

$$N = K \cdot \varepsilon_a^{-k} \quad (14)$$

with $k = 5$ and $K = 10^7$ is used, where ε_a refers to the amplitude of the strain hysteresis. The damage accumulation is then computed according to the elementary Palmgren-Miner rule [23], resulting in a fictitious

In order to assess the predictive performance of the regressor, two measures are taken into account. The coefficient of determination, also known as the R^2 error metric

$$R(y, y^*) = 1 - \frac{\sum_{i=1}^n (y_i - y_i^*)^2}{\sum_{i=1}^n (y_i - \bar{y})^2} \quad \text{with} \quad \bar{y} = 1/n \sum_{i=1}^n y_i, \quad (15)$$

describes the fraction of the variance in the observed data y which is explained by the model predictions y^* . It equals 1 for a perfect prediction and decreases with increasing deviations between y and y^* . In this application, the target y corresponds to the logarithmic fatigue damage sum $\lg D$ obtained from measurements, while y^* is the prediction prediction of the regression model, resulting from the reduced representation of acceleration measurements. Since R^2 is a very general regression metric, it does not differentiate between the prediction accuracy of smaller and larger fatigue damage sums. In order to capture how well the regression approach is suited for fatigue monitoring, the fatigue damage sum ratio

$$r_{\text{FDS}} = \frac{\sum_j D_j^*}{\sum_j D_j} \quad (16)$$

is introduced as a second metric. It compares the total sum of all n non-logarithmic fatigue damage contributions D_j in the testing dataset to the sum of their predictions D_j^* . For a perfect fatigue prediction, r_{FDS} equals 1, while a ratio of e.g. 2 means that the true fatigue damage sum is overestimated by a factor of 2.

4.2. Prediction of unlabeled data

Predicting the fatigue damage of unlabeled usage data is a very direct approach to fatigue monitoring. Evaluating the performance of a predictive model is increasingly difficult when many sensor channels, as well as multiple model variations are available. In order to provide a starting point for this evaluation, Figure 8 exemplarily displays the application of the presented approach to the fatigue damage prediction for strain sensor 1, using the scattering transform to compute the reduced representation of acceleration data. It can be seen that the fatigue damage from measurement and prediction are very strongly correlated, indicated by an R^2 value of 0.83. At the same time, both the general scatter and the error histogram indicate that errors in the range of ± 1 in $\lg D$, i.e., one decade in D , are relatively common. While the mean of the error is close to 0, the predictions D^* tend to be slightly larger than the computed values of D .

Given this baseline, the overall predictive performance on the unlabeled test dataset can be evaluated, which is presented in Figure 9. As stated in Section 3, strain sensors with very low amplitudes were omitted, as the corresponding locations are not relevant to fatigue and the measurements contain a significantly higher signal-noise-ratio. Regarding the R^2 plot, the regression setup using the scattering transform generally outperforms the approach based on the Fast Fourier transform significantly. This is reflected in a generally lower scatter in the prediction of individual data points, i.e., measurement sequences. Both approaches yield high overall R^2 -scores, averaging at roughly 0.85 for the scattering transform and 0.75 for the FFT. The fatigue damage sum ratio is generally more difficult to interpret, since high errors of individual predictions can compensate each other in the total damage sum. In this metric, the better approximation changes depending on the measurement location. Both approaches provide predictions which are mostly located in the range of $0.5 \leq r_{\text{FDS}} \leq 2$, meaning that the error of prediction is at most of factor 2, but the scattering based approach slightly underestimates the damage sum consistently.

4.3. Prediction of labeled data

The testing measurements of the labeled dataset can be used in order to evaluate how well the fatigue damage regression performs in more extreme cases. It contains measurements taken on both very even underground, as well as very uneven cobblestone. Many of these measurements are also recorded at very low riding speeds of 5 km/h to 15 km/h. Since no labeled data was used to parameterize the low dimensional representation or the regression model, it showcases the regression of events which are underrepresented in the unlabeled dataset.

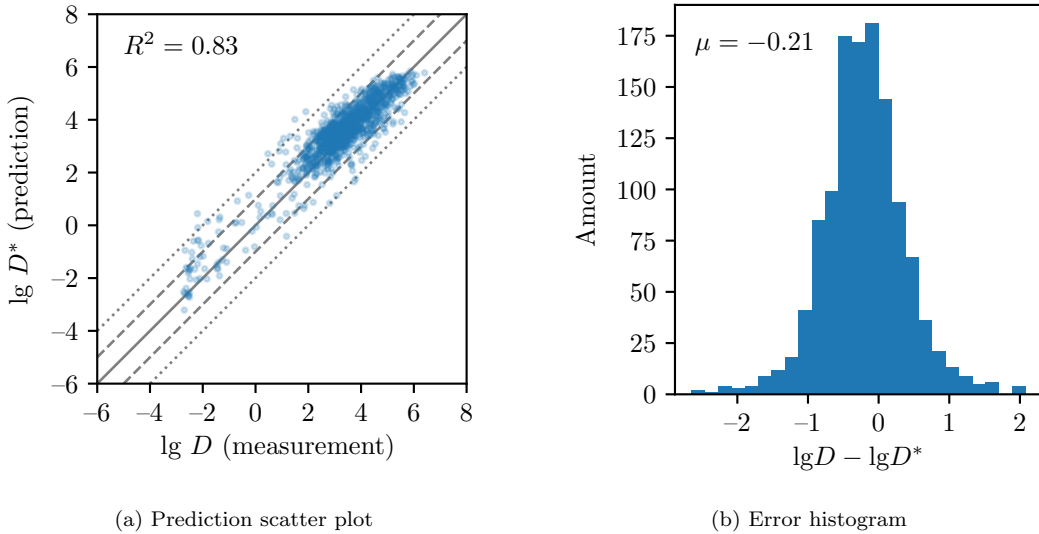


Figure 8: Fatigue damage sums D , computed from measurement samples at strain gauge 1, are compared to a prediction D^* , obtained from the low dimensional representation of concurrent acceleration measurements. All samples in the unlabeled testing dataset are shown. The grey middle line in the scatter plot (a) represents a perfect prediction, while the dashed lines each denote an error of 1 in the prediction of $\lg D$, corresponding to an error of factor 10 in D . The prediction error (b) is slightly biased towards overprediction.

In Figure 10, the results of labeled data predictions are shown, grouped by even and uneven undergrounds. Compared to the unlabeled data, the general predictive accuracy decreases significantly for both scattering transform and FFT, indicated by the generally lower R^2 score. Especially strain sensor 11 is predicted extremely poorly by both models. Apart from this sensor, both approaches yield relatively similar results on even underground, while the scattering transform scores consistently higher results on the uneven cobblestone. This trend is also reflected in the fatigue damage sum ratio, where all scattering results are in the range of $0.5 \leq r_{\text{FDS}} \leq 2$, while the fatigue damage on cobblestone is overestimated consistently by the Fast Fourier based model.

5. Maneuver identification

In Section 4, a strong correlation between the reduced representation of acceleration data and the fatigue damage accumulation was shown. Maneuver identification is an alternative approach to direct fatigue damage regression, where the aim is to correctly identify the current dynamic state of the vehicle. This information can afterwards be used to associate each maneuver with a corresponding damage accumulation model, but it can also provide general usage statistics to vehicle design engineers or fleet managers. The aim of this section is to show how the proposed low dimensional data representation can be used to identify maneuvers by providing a discrete classification example.

5.1. Semi-supervised parameterization

A main difficulty with classification tasks is the collection of labeled data examples. In order for a data-driven algorithm to identify a specific maneuver of interest, examples of this maneuver have to be provided. This process can be very cost intensive, since the corresponding data has to be either collected in targeted maneuver measurements or manually extracted from general usage data, for example by using rider logs of each measurement or video recordings. As a result, labeled data is rarely available in large quantities, which should be taken into account when developing a maneuver identification algorithm.

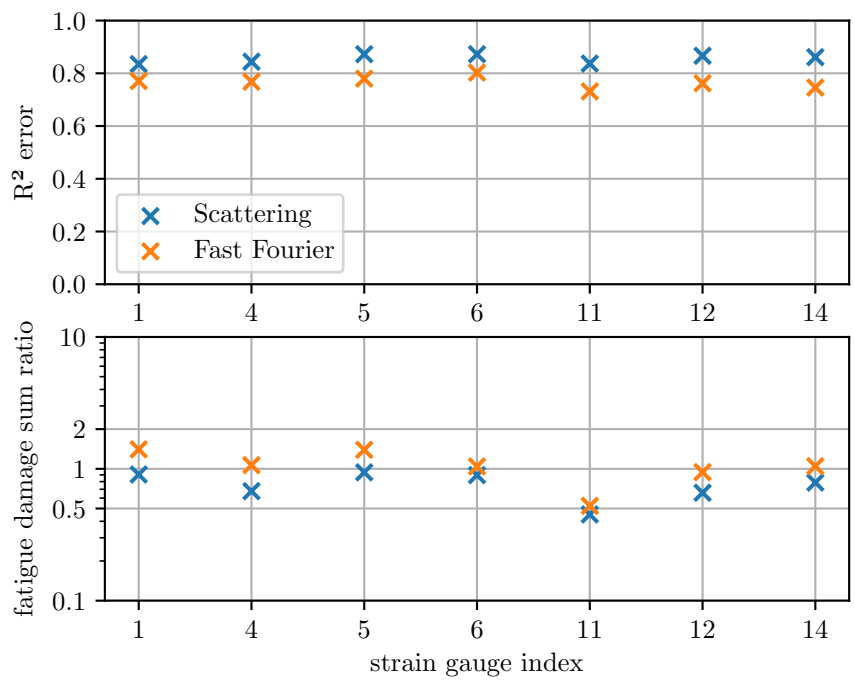


Figure 9: The low dimensional representation of acceleration sensor data is used to predict the fatigue damage sum of the corresponding strain measurements for all samples in the unlabeled testing dataset. Only strain sensors with comparatively high average amplitudes are shown.

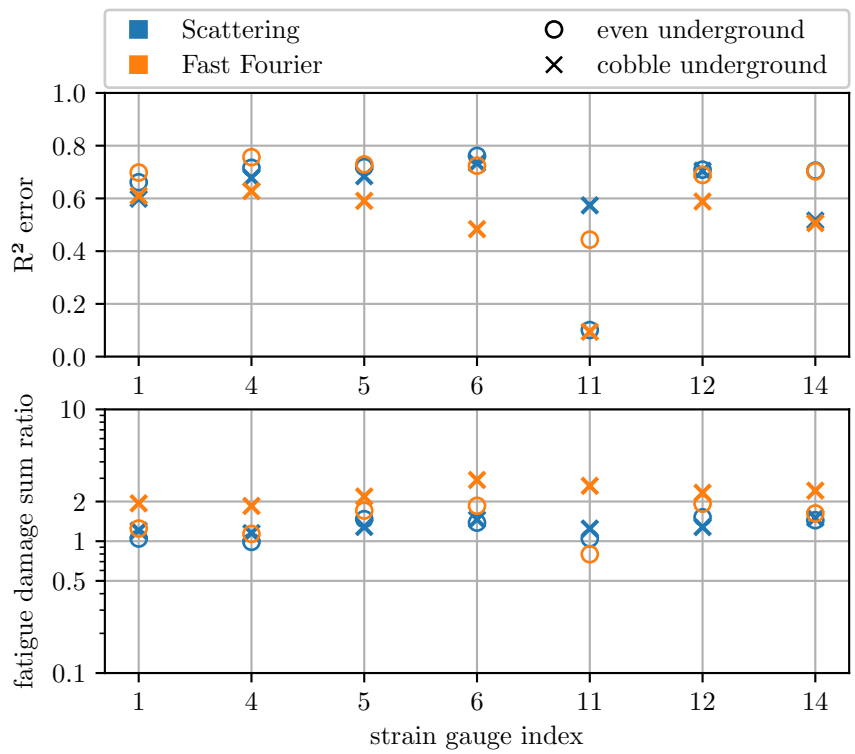


Figure 10: The low dimensional representation of acceleration sensor data is used to predict the fatigue damage sum of the corresponding strain measurements for all samples in the labeled testing dataset. The data samples are divided into even underground, and very uneven cobblestone underground. Only strain sensors with comparatively high average amplitudes are shown.

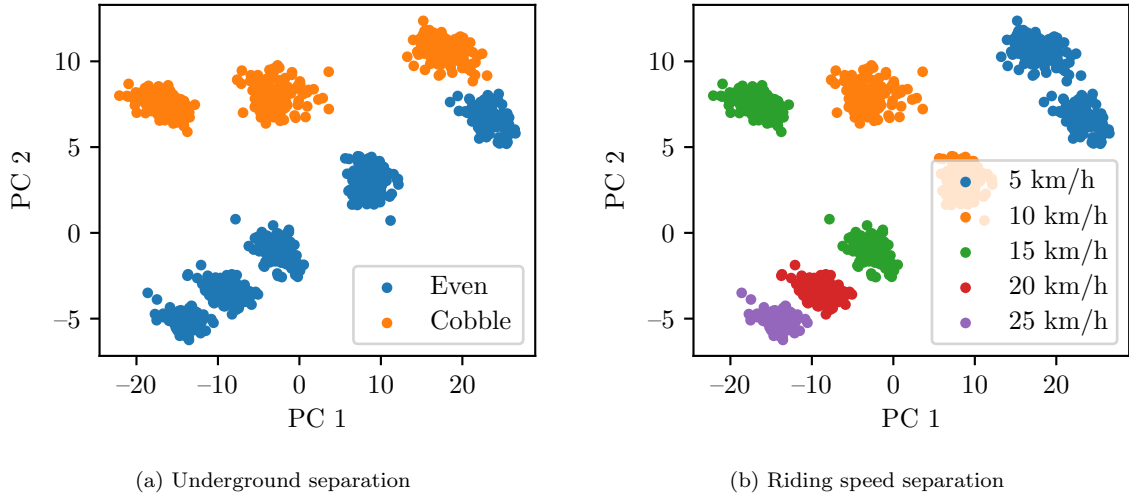


Figure 11: Using the training portion of the labeled dataset, the location of specific maneuvers in the principal component space can be identified. Even and uneven undergrounds (a) can be separated mostly along PC 2, while a decrease in PC 1 corresponds to an increase in riding speed (b).

Since maneuver data should be collected from all vehicles in a fleet, only the acceleration sensors of the eBike setup, presented in Subsection 3.1, are used in this study. From the acceleration data, the reduced representation is build exactly as described in Subsection 4.1. First, the data is split into segments, then either the scattering or Fast Fourier transform is applied and finally, the PCA is used to reduce the dimensionality. This process uses only unlabeled usage data, which is generally easy to obtain.

This approach is referred to as semi-supervised, since on one hand, no labeled data is required to obtain the PC scores from acceleration measurements, but on the other hand, some labeled examples are still required to physically interpret the PC scores and to link them to specific maneuvers. This is achieved using the training examples from the labeled dataset. Figure 11 shows that principal components 1 and 2 contain a lot of information on the riding underground and speed. In the underground separation plot (a), all examples of the uneven underground are located in the left branch and the examples of even undergrounds are clustered on the right. As a result, it is very easy for a classification algorithm to correctly classify the underground from the data, for example by placing a decision boundary in between both categories. From the riding speed separation plot (b), it can be concluded that an increasing riding speed is reflected by a decrease in PC 1. The speed could therefore be classified into bins of measured speeds depending on a corresponding principal component range. While information about the rider of each labeled measurement and their respective weight is available in the dataset, no combination of two principal components was found which clearly separates these classes visually.

5.2. Discrete maneuver classification example

With the knowledge that underground and speed information are available in the principal component space, a classification model can be created, which predicts labels from PC scores. These labels can be categorical, e.g. even or cobblestone underground, discrete numerical, e.g. 10 km/h or 15 km/h, or a combination of both, e.g. rider 1 with weight 66 kg or rider 2 with weight 83 kg. For this model, a k -Nearest-Neighbors classifier [24] is chosen, where the label of a new example is predicted based on the most common labels among its k nearest neighboring points, selected using the euclidean norm over all 10 principal component axes. The parameter $k = 20$ was selected arbitrarily based on the total number of points in the training dataset. In more complex classification tasks, it can be estimated using cross validation

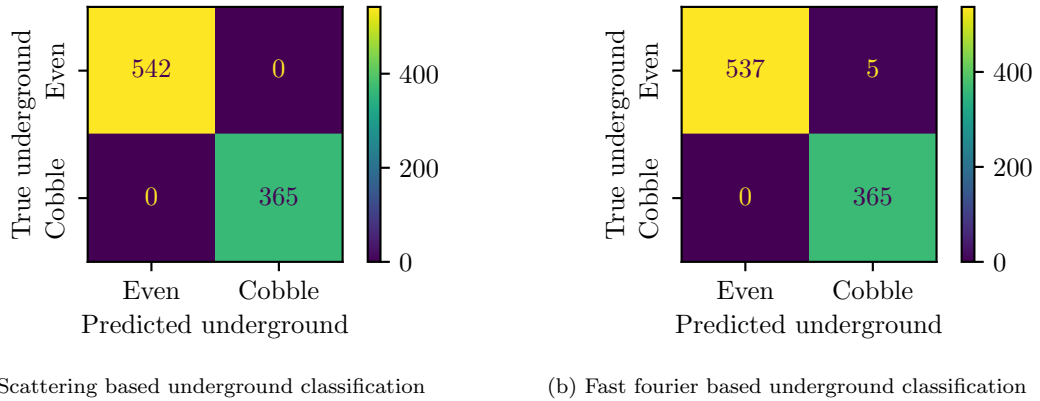


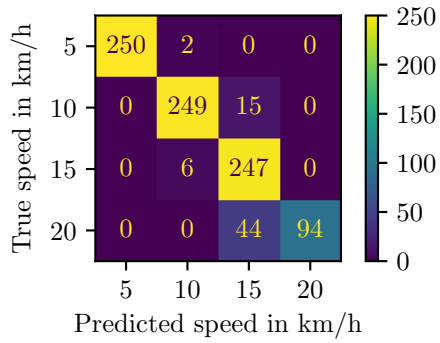
Figure 12: Using the scattering transform based representation, the underground is classified with a perfect accuracy of 100 %, while the fast Fourier transform leads to an almost perfect accuracy of 99.5 %.

[24]. Once the classification model is parameterized, it is employed to predict all examples from the labeled testing dataset. Again, a comparison is made between the reduced acceleration representation based on the scattering transform and the Fast Fourier transform.

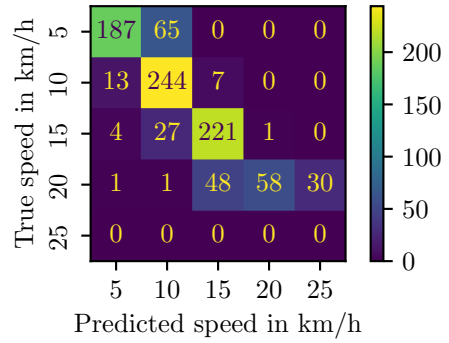
The underground classification results are depicted as a confusion matrix in Figure 12. It shows that the scattering based classifier is able to perfectly predict all undergrounds, while the Fast Fourier based classifier reaches an almost perfect accuracy of 99.5 %. Figure 13 shows the classification of riding speed categories. Here, the scattering based approach yields an accuracy of 92.6 %, while the Fast Fourier based model only reaches 78.3 %. It is also worth noting that for even underground data, training data of up to 25 km/h is available, while the testing dataset only includes examples up to 20 km/h, resulting from a different measuring location. While the scattering based approach never falsely classifies a testing sample as 25 km/h, this problem occurs for the Fast Fourier based classifier. For the last classification case, Figure 14 shows the rider classification results. Here, the Fast Fourier based model outperforms the Scattering transform with a near perfect accuracy of 98.7 % compared to 90.9 %.

6. Conclusions

This paper shows how fatigue monitoring for vehicle fleets can be achieved by a combination of feature extraction and dimensionality reduction, using a reduced sensor setup. This is achieved by a reference approach, where all vehicles in a fleet have a given set of standard acceleration sensors, which are used to identify the dynamic state of the vehicle. These standard measurements are extended by additional reference sensors, which only have to be installed at one reference vehicle and provide local strain responses, necessary for the fatigue assessment. A sensor equipped eBike served as the demonstrator for this approach, which was used to obtain an unlabeled and a labeled dataset for model parameterization and validation. A low dimensional representation of the acceleration measurements constitutes the core of both application cases. In the first study, it was shown that a strong correlation between the reduced acceleration data representation the fatigue damage sums of concurrent strain measurements exist, which was subsequently used in a fatigue damage regression. The second application used a semi-supervised approach to physically interpret the principal component scores in the reduced representation, enabling a maneuver classification. Two methods for feature extraction, namely the scattering transform and the Fast Fourier transform, were compared in multiple applications, while principal component analysis was used for the dimensionality reduction task. The scattering transform outperformed the FFT based model in most regression examples, yielding more accurate fatigue damage predictions per time sequence in unlabeled and labeled datasets. In the maneuver identification tasks, both models classified the underground very well and the scattering

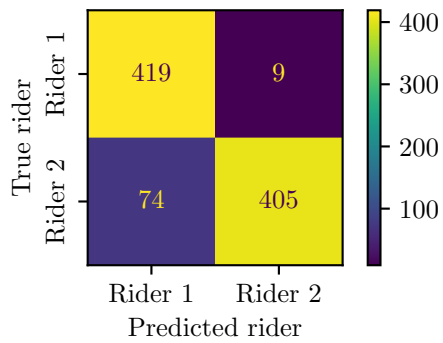


(a) Scattering based speed classification

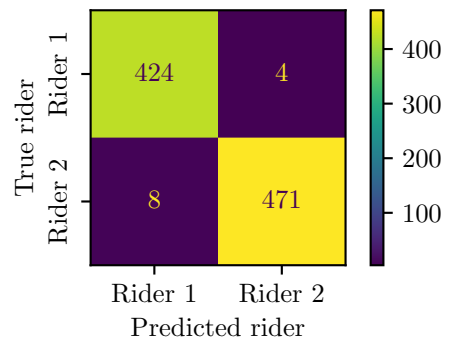


(b) Fast Fourier based speed classification

Figure 13: Using the scattering transform, the riding speed can be classified with an accuracy of 92.6%. Here, no samples are incorrectly classified by more than one class and the erroneous samples are mostly samples at 20 km/h that are falsely classified as 15 km/h. Using the fast Fourier based representation, falsely classified samples exist between all classes, leading to an accuracy of only 78.3%. Since samples of 25 km/h exist in the even underground training data, but not in the testing data, some samples with a speed of 20 km/h are incorrectly attributed to this range for the Fast Fourier based representation, but not for the Scattering based variant.



(a) Rider classification scattering



(b) Rider classification fast fourier

Figure 14: The rider classification based on the scattering representation achieves an accuracy of 90.9%, with most incorrect predictions stemming from measurement data of rider 2. The fast Fourier based representation yields a near perfect accuracy of 98.7%, where false predictions are evenly distributed between both riders.

transform outperformed the Fast Fourier based model in terms of driving speed estimation, while falling short in the rider category.

The presented approach is fundamentally designed to be parameterized using only measurement data and therefore does not require a finite element solution to function. Still, information from an FE model can contribute to the accuracy of this approach by identifying fatigue critical strain sensor locations from simple load cases, or through analysing mode shapes in order to find anti-nodes to position acceleration sensors. Unfortunately, no FE model of the eBike was available at the time of sensor placement in this study, therefore further improvements can be expected by taking such information into account.

While a fictitious WÖHLER-curve is sufficient for demonstrating that fatigue damage contributions from measurements can be correctly reproduced by a predictive regression model, further care is required in the deployment of such a fatigue monitoring approach. When a local WÖHLER-curve is available for the monitored strain positions, it might be useful to incorporate an additional correction factor into the regressor in order to ensure that predicted damage sums are unbiased. The corresponding correction factor can be identified using cross validation on the training dataset. In cases where a local WÖHLER-curve is not available, fictitious damage sums can be interpreted as fatigue indicators, which steadily increases with vehicle usage. If the corresponding fleet is sufficiently large, these indicator values can be correlated with actual component failures which are observed during maintenance, leading to a monitoring strategy that automatically improves in accuracy over time.

In the maneuver identification section, it was shown that labeled data can be used to identify a given set of predefined maneuvers. This was mainly done to show that maneuver information is accessible through the reduced acceleration data representation, but might be unsatisfactory when the expected number of relevant maneuvers is very high. In this case, it might be feasible to use clustering techniques like k-means clustering or gaussian mixture models to automatically identify clusters from unlabeled data. This approach might be especially promising when large differences in the overall system behavior are expected between different maneuvers.

In order to apply the presented approach to a vehicle fleet, special care has to be taken regarding the precise sensor positioning and calibration, as well as manufacturing tolerances between different vehicles. The evaluation of these influences is subject of further investigation.

7. Declaration of Competing Interest

The authors declare that they have no known competing financial interests or personal relationships that could have appeared to influence the work reported in this paper.

8. Acknowledgments



This measure is co-financed with tax revenues on the basis of the budget adopted by the members of the Saxon State Parliament.

The authors gratefully acknowledge the GWK support for funding this project by providing computing time through the Center for Information Services and HPC (ZIH) at TU Dresden.

References

- [1] M. Burger, K. Dreßler, M. Speckert, Load assumption process for durability design using new data sources and data analytics, *International Journal of Fatigue* 145 (2021) 106116. doi:10.1016/j.ijfatigue.2020.106116. URL <https://linkinghub.elsevier.com/retrieve/pii/S0142112320306484>

- [2] J. Brownjohn, Structural health monitoring of civil infrastructure, *Philosophical Transactions of the Royal Society A: Mathematical, Physical and Engineering Sciences* 365 (1851) (Brownjohn2007) 589–622. doi:10.1098/rsta.2006.1925. URL <https://royalsocietypublishing.org/doi/10.1098/rsta.2006.1925>
- [3] M. Flah, I. Nunez, W. Ben Chaabene, M. L. Nehdi, Machine Learning Algorithms in Civil Structural Health Monitoring: A Systematic Review, *Archives of Computational Methods in Engineering* 28 (4) (Flah2021) 2621–2643. doi:10.1007/s11831-020-09471-9. URL <https://link.springer.com/10.1007/s11831-020-09471-9>
- [4] E. Haibach, *Betriebsfestigkeit: Verfahren und Daten zur Bauteilberechnung*, VDI-Buch, Springer, 2002. URL https://books.google.de/books?id=vwZ_U6eTcycC
- [5] S. Stellmach, L. Braun, M. Wächter, A. Esderts, S. Dieckhaus, On load assumptions for self-propelled forage harvesters, *International Journal of Fatigue* 147 (2021) 106114. doi:10.1016/j.ijfatigue.2020.106114. URL <https://linkinghub.elsevier.com/retrieve/pii/S0142112320306460>
- [6] J. P. Quigley, Y.-L. Lee, L. Wang, Review and Assessment of Frequency-Based Fatigue Damage Models, *SAE International Journal of Materials and Manufacturing* 9 (3) (2016) 565–577. doi:10.4271/2016-01-0369. URL <https://www.sae.org/content/2016-01-0369/>
- [7] R. C. Ugras, O. K. Alkan, S. Orhan, M. Kutlu, A. Mugan, Real time high cycle fatigue estimation algorithm and load history monitoring for vehicles by the use of frequency domain methods, *Mechanical Systems and Signal Processing* 118 (2019) 290–304. doi:10.1016/j.ymsp.2018.08.043. URL <https://linkinghub.elsevier.com/retrieve/pii/S088832701830582X>
- [8] H. Hjeltn, R. Brincker, J. Graugaard-Jensen, K. Munch, Determination of stress histories in structures by natural input modal analysis, *Proceedings of IMAC-XXIII, A Conference & Exposition on Structural Dynamics*.
- [9] M. Tarpø, B. Nabuco, C. Georgakis, R. Brincker, Expansion of experimental mode shape from operational modal analysis and virtual sensing for fatigue analysis using the modal expansion method, *International Journal of Fatigue* 130 (2020) 105280. doi:10.1016/j.ijfatigue.2019.105280. URL <https://linkinghub.elsevier.com/retrieve/pii/S0142112319303846>
- [10] V. Flores Terrazas, O. Sedehi, C. Papadimitriou, L. S. Katafygiotis, A streamline approach to multiaxial fatigue monitoring using virtual sensing, *Structural Control and Health Monitoring* 29 (1). doi:10.1002/stc.2863. URL <https://onlinelibrary.wiley.com/doi/10.1002/stc.2863>
- [11] V. Rouss, W. Charon, G. Cirrincione, Neural model of the dynamic behaviour of a non-linear mechanical system, *Mechanical Systems and Signal Processing* 23 (4) (2009) 1145–1159. doi:https://doi.org/10.1016/j.ymsp.2008.09.004. URL <https://www.sciencedirect.com/science/article/pii/S0888327008002215>
- [12] J. Kullaa, Combined empirical and analytical virtual sensing in structural dynamics for uncertainty reduction, in: *Proceedings of the 1st International Conference on Uncertainty Quantification in Computational Sciences and Engineering (UNCECOMP 2015)*, Institute of Structural Analysis and Antiseismic Research School of Civil Engineering National Technical University of Athens (NTUA) Greece, Crete Island, Greece, 2015, pp. 443–466. doi:10.7712/120215.4284.564. URL <http://www.eccomasproceedia.org/conferences/thematic-conferences/uncecomp-2015/4284>
- [13] J. Kullaa, Bayesian virtual sensing in structural dynamics, *Mechanical Systems and Signal Processing* 115 (2019) 497–513. doi:10.1016/j.ymsp.2018.06.010. URL <https://linkinghub.elsevier.com/retrieve/pii/S0888327018303467>
- [14] X. Wang, D. Yang, Y. Wang, H. Guo, N. Liu, W. Li, Time-domain signal reconstruction of vehicle interior noise based on deep learning and compressed sensing techniques, *Mechanical Systems and Signal Processing* 139 (2020) 106635. doi:10.1016/j.ymsp.2020.106635. URL <https://linkinghub.elsevier.com/retrieve/pii/S0888327020300212>
- [15] J. Bruna, S. Mallat, Audio Texture Synthesis with Scattering Moments, arXiv:1311.0407 [cs, stat] (Nov. 2013). URL <http://arxiv.org/abs/1311.0407>
- [16] J. Anden, S. Mallat, Deep Scattering Spectrum, *IEEE Transactions on Signal Processing* 62 (16) (2014) 4114–4128. doi:10.1109/TSP.2014.2326991. URL <http://ieeexplore.ieee.org/document/6822556/>
- [17] S. Mallat, Understanding deep convolutional networks, *Philosophical Transactions of the Royal Society A: Mathematical, Physical and Engineering Sciences* 374 (2065) (2016) 20150203. doi:10.1098/rsta.2015.0203. URL <https://royalsocietypublishing.org/doi/10.1098/rsta.2015.0203>
- [18] L. Seydoux, R. Balestriero, P. Poli, M. d. Hoop, M. Campillo, R. Baraniuk, Clustering earthquake signals and background noises in continuous seismic data with unsupervised deep learning, *Nature Communications* 11 (1) (2020) 3972. doi:10.1038/s41467-020-17841-x. URL <https://www.nature.com/articles/s41467-020-17841-x>
- [19] M. Andreux, T. Angles, G. Exarchakis, R. Leonarduzzi, G. Rochette, L. Thiry, J. Zarka, S. Mallat, J. andén, E. Belilovsky, J. Bruna, V. Lostanlen, M. Chaudhary, M. J. Hirn, E. Oyallon, S. Zhang, C. Cella, M. Eickenberg, Kymatio: Scattering Transforms in Python, arXiv:1812.11214 [cs, eess, stat] (May 2022). URL <http://arxiv.org/abs/1812.11214>
- [20] I. Jolliffe, *Principal Component Analysis*, 2nd Edition, Springer-Verlag New York, 2002.
- [21] F. Pedregosa, G. Varoquaux, A. Gramfort, V. Michel, B. Thirion, O. Grisel, M. Blondel, P. Prettenhofer, R. Weiss, V. Dubourg, J. Vanderplas, A. Passos, D. Cournapeau, M. Brucher, M. Perrot, E. Duchesnay, Scikit-learn: Machine Learning in Python, *Journal of Machine Learning Research* 12 (2011) 2825–2830.
- [22] C. McInnes, P. Meehan, Equivalence of four-point and three-point rainflow cycle counting algorithms, *International Journal of Fatigue* 30 (3) (2008) 547–559. doi:https://doi.org/10.1016/j.ijfatigue.2007.03.006.

URL <https://www.sciencedirect.com/science/article/pii/S0142112307001119>

- [23] A. Palmgren, Die Lebensdauer von Kugellagern, Zeitschrift des Vereines Deutscher Ingenieure 68 (14) (1924) 339–341.
- [24] G. James, D. Witten, T. Hastie, R. Tibshirani, An Introduction to Statistical Learning, 2nd Edition, Springer New York, NY, 2013.